AIAA JOURNAL
Vol. 61, No. 4, April 2023

Effects of Dilution and Pressure on Detonation Propagation Across an Inert Layer

Yuan Wang* and Jingyi Su*
Peking University, 100871 Beijing, People's Republic of China
Ralf Deiterding†
University of Southampton, Southampton, England SO16 7QF, United Kingdom
and
Zheng Chen‡
Peking University, 100871 Beijing, People's Republic of China

https://doi.org/10.2514/1.J062397

In explosion accidents, inert layer(s) can be used to dampen or suppress detonation propagation. In detonation engines, the detonation may propagate in an inhomogeneous mixture with inert layer(s). Here, the detonation propagation in hydrogen/oxygen/nitrogen mixtures with a single inert layer normal to the detonation propagation direction was investigated. Six hydrogen/oxygen/nitrogen mixtures with different amounts of nitrogen dilution and at different initial pressures were considered. The emphasis was placed on assessing the effects of nitrogen dilution and pressure on detonation across an inert layer. It was found that successful detonation reinitiation occurs only when the inert layer thickness is below some critical value. The detonation reinitiation process was analyzed. The interactions of transverse waves, the reactive–inert layer interface, and instabilities jointly induced local autoignition/explosions and detonation reinitiation. Counterintuitively, it was found that a thicker inert layer is required to quench a weaker detonation (with more nitrogen dilution or with lower-energy density at lower pressure). With the increase of nitrogen dilution or the decrease of initial pressure, the induction length and cell size of the detonation became larger, which unexpectedly resulted in the larger critical inert layer thickness.

I. Introduction

As a zero-carbon-emission fuel, hydrogen has recently drawn significant attention due to its promising applications in energy storage and energy conversion [1]. Great effort has been devoted to investigating the properties of hydrogen flames and detonations (e.g., Refs. [2–8]). However, there is still severe safety concern for hydrogen storage and utilization because hydrogen is easily ignited [9–11]. It is well known that accidental explosion can cause extremely severe damage if detonation occurs. One way to reduce the damage is to dampen or suppress detonation propagation in combustible gases using inert zones or inert layers. Transition of detonation across an inert region might induce detonation quenching and reinitiation. Besides, hydrogen is popularly used in rotating detonation engines (RDEs). In RDEs, hydrogen and air may not be perfectly mixed; and a burned mixture can appear in front of the detonation front. Therefore, understanding detonation propagation and quenching in inhomogeneous hydrogen/oxygen/diluent mixtures is of crucial importance for controlling explosion and developing detonation engines. In the literature, there are many studies on detonation propagation in inhomogeneous mixtures (see Ref. [12]). In this work, we specifically focus on the transition of gaseous detonation across a single inert layer normal to the detonation propagation direction in different hydrogen/oxygen/nitrogen ($H_2/O_2/N_2$) mixtures.

There are several experimental or numerical studies on/related to detonation propagation across a single or multiple inert layers. For example, Teodorczyk and Benoan [13] studied detonation reinitiation after the interaction of detonation with an inert zone. Bull et al. [14] investigated detonation propagation in ethylene/air and propane/air mixtures with an inert zone consisting of pure air. They measured the critical size of the inert zone and the transition distance for detonation reinitiation. Bjerketvedt et al. [15] conducted experiments on detonation reinitiation across a single inert region and assessed different factors affecting the detonation reinitiation. Tropin and Bedarev [16] investigated numerical detonation suppression by an inert layer with different inert gases. They found that carbon dioxide is more efficient for suppressing the detonation wave than nitrogen and argon. Tang-Yuk et al. [17] simulated detonation transmission across an inert layer and found that the critical inert layer thickness for the two-dimensional (2-D) case was one order larger than that for the one-dimensional (1-D) case. In a recent study by Wang et al. [18], detonation propagation across multiple inert layers was simulated and a double cellular structure was observed and interpreted. The size of the large cellular structure was found to be linearly proportional to the inert layer spacing.

Although detonation propagation across an inert layer(s) was investigated in the aforementioned studies, the reinitiation mechanism and the dependence of critical inert layer thickness on mixture composition and thermal conditions are still not well understood. This motivates the present study, for which the objectives are twofold: 1) to interpret the mechanism and critical condition for detonation reinitiation after it is quenched by an inert layer, and 2) to assess the effects of nitrogen dilution and pressure on detonation across an inert layer. We shall consider detonation propagation in different $H_2/O_2/N_2$ mixtures with a single inert layer normal to the detonation propagation direction. A single inert layer instead of multiple inert layers is considered here so that complicated interactions between detonation and multiple inert layers are prevented, and thereby the detonation reinitiation mechanism can be clearly interpreted. Both 1-D and 2-D simulations are conducted. Detailed chemistry is considered in all simulations.

In the following sections, the model and the numerical methods are introduced first. Then, the results from 1-D and 2-D simulations are presented, and detonation reinitiation as well as its dependence on dilution and pressure are discussed. Finally, the conclusions are summarized.

Received 31 August 2022; revision received 19 November 2022; accepted for publication 8 December 2022; published online 26 December 2022.

*Graduate Student, College of Engineering, Center for Applied Physics and Technology, State Key Laboratory for Turbulence and Complex Systems.
†Professor, Aerodynamics and Flight Mechanics Research Group.
‡Professor, College of Engineering, Center for Applied Physics and Technology, State Key Laboratory for Turbulence and Complex Systems; cz@pku.edu.cn (Corresponding Author).

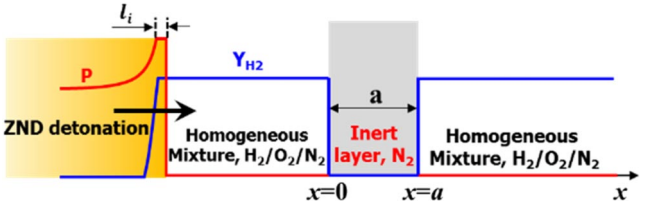

Fig. 1 Schematic of the initial pressure and hydrogen mass fraction distributions.

II. Model and Numerical Methods

The model is depicted in Fig. 1. The detonation propagates into a static, homogeneous, stoichiometric $H_2/O_2/N_2$ mixture, which is separated by an inert layer of pure nitrogen. The inert layer starts at $x = 0$ cm and ends at $x = a$. The Zel'dovich-von Neumann-Doering (ZND) detonation structure with the induction length of l_i is used to initiate the detonation propagating to the right side. For the 2-D case, the detonation cellular structure fully develops before the detonation enters the inter layer.

The detonation is quenched after entering the inert layer, and the leading shock is attenuated during its propagation across it. When the inert layer thickness is below some critical value, denoted as a_c, the detonation can be reinitiated by the transmitted shock. The critical inert layer thickness a_c is expected to be related to the induction length l_i and the detonation cell size λ, respectively, for 1-D and 2-D detonations. Note that the induction length and the cell size are obtained, respectively, from the present 1-D and 2-D simulations. To change l_i and λ, we considered different stoichiometric $H_2/O_2/N_2$ mixtures (for which the molar ratio is $H_2:O_2:N_2 = 2:1:s$) with different amounts of N_2 dilution of $s = 3.76$, 5, 6, and 7 and at different initial pressures of $P_0 = 15$, 30 and 60 KPa (see Table 1).

Table 1 lists six mixtures considered in this work. The induction length l_i and detonation cell size λ for these mixtures are also listed in Table 1. The induction length is defined as the distance from the leading shock wave to the position where maximum thermicity appears. The cell size is the vertical length of the regular detonation cell structure. As expected, Table 1 shows that increasing nitrogen dilution and reducing initial pressure can both greatly increase the induction length and detonation cell size.

The in-house codes A-SURF [19,20] and AMROC [21,22] were used to simulate 1-D and 2-D detonations propagating across an inert layer, respectively. Both codes solve the Navier–Stokes equations for unsteady, compressible, multicomponent, reactive flow using the finite volume method. The Harten–Lax–van Leer contact (HLLC) or hybrid Roe–Harten–Lax–van Leer (HLL) Riemann solver for mixtures of thermally perfect gases was used to calculate the convective fluxes. The second-order-accurate central difference scheme was used for multispecies diffusion terms. The detailed kinetic model for hydrogen oxidation developed by Li et al. [23] was used in all simulations. The CHEMKIN package was employed to evaluate the reaction rates and thermodynamic properties. Both A-SURF and AMROC have been successfully used in previous studies on detonation propagation (e.g., Refs. [24–30]). The details on the governing equations, numerical methods, and code validation of A-SURF and AMROC can be found in Refs. [19–21], and are thereby not repeated here.

Table 1 Composition, initial temperature and pressure, induction length, and detonation cell size of six mixtures

No.	$H_2:O_2:N_2$	T_0, K	P_0, kPa	l_i, mm	λ, mm
1	2:1:3.76	300	15	1.49	12
2	2:1:5	300	15	2.22	14.3
3	2:1:6	300	15	3.08	20
4	2:1:7	300	15	4.31	25
5	2:1:7	300	30	2.23	13.3
6	2:1:7	300	60	1.29	7.5

Transmissive boundary conditions were used for the left and right sides in both 1-D and 2-D computational domains. Periodic boundary conditions were used for the top and bottom sides in the 2-D simulations. Therefore, the effects of any boundary layer and its interaction with shock waves were not considered here. Note that, in practice, detonation propagates in a finite domain with physical confinement rather than in an infinite domain with periodic boundary conditions. This study focused on the effect of single inert layer, and therefore the confinement effect was not considered here for simplicity. In future works, it would be interesting to take into account the confinement effect.

The length and width of the computational domain are large enough for detonation propagation and formation of a steady cellular structure. To accurately and efficiently resolve the transient process, a dynamically adaptive mesh refinement was used in both 1-D and 2-D simulations. Mesh refinement is based on local gradients of temperature, density, and pressure. The finest mesh size is 7.8 μm. Because the smallest induction length is $l_i = 1.29$ mm, there are more than 165 grid points within one induction length. Our numerical tests indicated that the conclusions remained the same when the finest mesh size was halved. Compared to the present work, some studies [31,32] showed that the relatively coarser mesh resolutions were able to adequately capture the detonation wave dynamics in detonation engines.

III. Results and Discussion

Both 1-D and 2-D simulations were conducted. In practice, the detonation propagation process is intrinsically multidimensional. Therefore, the 1-D simulation cannot reveal the real dynamics of the detonation wave. Nevertheless, the 1-D simulation is still helpful in understanding the coupling between the lead shock and the reactions, at least in a qualitatively manner. Therefore, the results from the 1-D simulation are first presented and discussed in the following.

A. One-Dimensional Detonation Propagation

First, we considered 1-D detonation propagating across an inert layer for the six mixtures listed in Table 1. Only the results for mixture 1 and mixture 4 are shown in Fig. 2. The vertical dashed lines represent the left and right boundaries of the inert layer at $x = 0$ and $x = a$.

In simulation, the shock position is determined based on the maximum pressure gradient, and the shock speed is obtained via numerical differentiation of the shock position with respect to time. Figure 2a shows that the shock speed decays rapidly after it enters the inert layer starting at $x = 0$ cm. Within the inert layer, the shock speed decreases from the Chapman-Jouguet (CJ) detonation speed $D_{CJ} = 1695$ to 1578 m/s (i.e., $0.93D_{CJ}$) for $a = 5$ mm and to 1521 m/s (i.e., $0.90D_{CJ}$) for $a = 8$ mm, respectively. Successful detonation reinitiation is achieved only for $a = 5$, 6, and 7 mm. Similar to the direct detonation initiation observed in previous studies (e.g., Refs. [33–35]), for successful detonation reinitiation, an overdriven detonation develops after a rapid decrease in the leading shock speed. Then, the overdriven detonation decays toward the CJ detonation. With the increase of inert layer thickness, the position for successful detonation reinitiation and the maximum speed of the overdriven detonation both become larger. However, further increasing the inert layer thickness to $a = 8$ mm results in the failure of the detonation reinitiation, and thereby continuous decay of the leading shock speed. This is because the strength of the transmitted shock becomes too weak to trigger local autoignition and overdriven detonation afterward for relatively large inert layer thickness. The aforementioned evolution of the leading shock speed is consistent with the idealized detonation reinitiation process across an inert layer presented in Ref. [13].

Similar results are observed in Fig. 2b for mixture 4. Compared to mixture 1, mixture 4 has much higher N_2 dilution, and thereby weaker detonation strength. However, Figs. 2a and 2b show that the critical inert layer thickness of mixture 4 is larger than that for mixture 1. This is counterintuitive because a weaker detonation is expected to be quenched by a thinner inert layer. Table 1 shows that the induction lengths of mixture 1 and mixture 4 are, respectively,

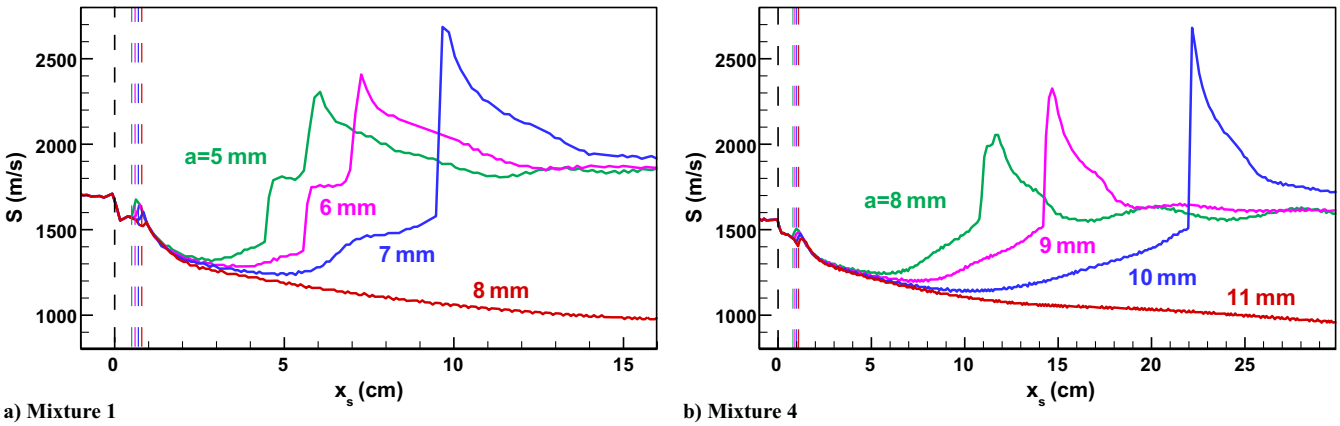

a) Mixture 1 b) Mixture 4

Fig. 2 Change of the leading shock speed with its position for mixtures 1 and 4.

$l_i = 1.49$ mm and $l_i = 4.31$ mm. The results in Fig. 2 indicate that a_c increases with l_i. Therefore, reinitiation for detonation propagating across an inert layer is more closely related to the induction length than the detonation strength.

Figure 3 shows the details on the detonation transmission involving shock–reaction decoupling, local autoignition, and detonation reinitiation. The gray zone in Fig. 3 corresponds to the inert layer. Moreover, Fig. 3 shows different states: zone I denotes steady detonation

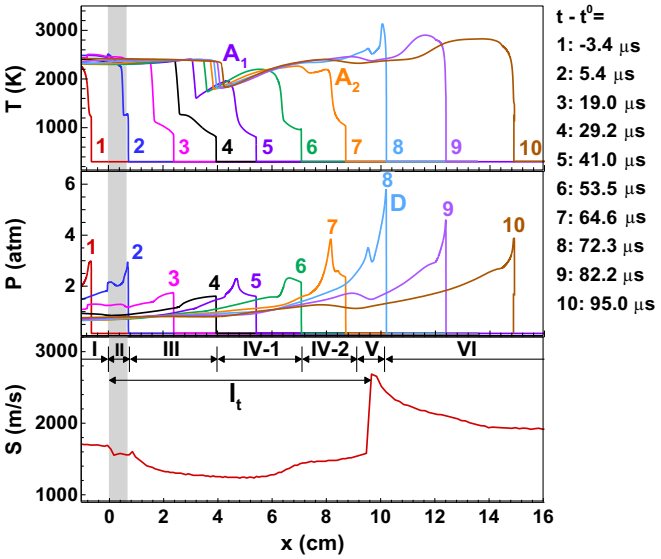

a) Mixture 1, a=7 mm

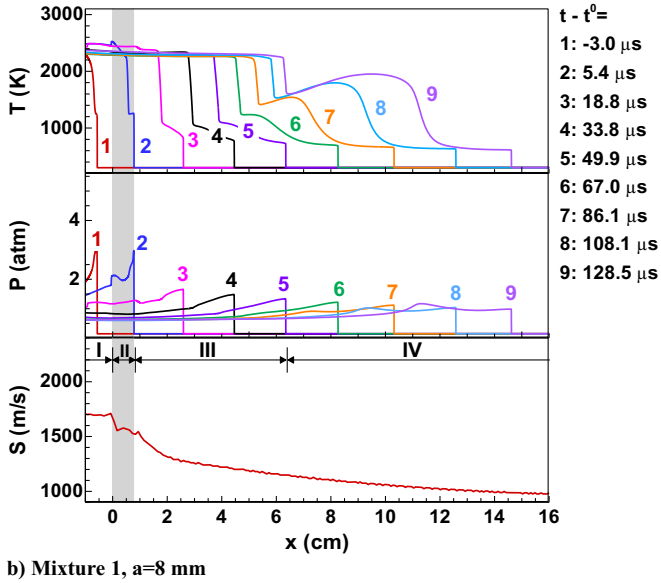

b) Mixture 1, a=8 mm

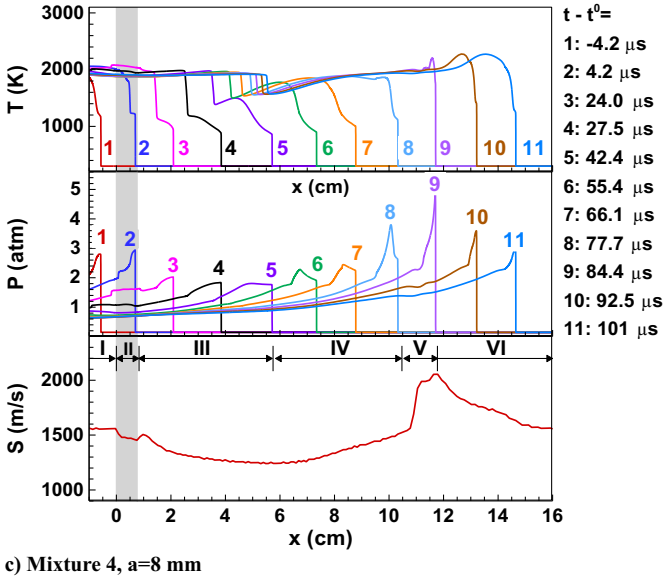

c) Mixture 4, a=8 mm

Fig. 3 Temporal evolution of temperature and pressure distributions as well as leading shock speed.

propagation; zone II denotes detonation quenching in the inert layer; zone III denotes shock attenuation; zone IV-1 denotes first autoignition; zone IV-2 denotes second autoignition; zone V denotes development of overdriven detonation; and zone VI denotes transition to steady detonation propagation. In Fig. 3, A_1 represents the first autoignition, A_2 represents the second autoignition, and D represents detonation.

Figure 3a shows that for mixture 1 with $a = 7$ mm (corresponding to the blue line in Fig. 2a), after entering the inert layer, shock–reaction decoupling is observed at $t - t^0 = 5.4$ μs (line 2 in Fig. 3a). Here, t^0 represents the time when the detonation enters the inert layer at $x = 0$ cm. The distance between the leading shock and the reaction front further increases and reaches its maximum value of 14.1 mm at $t - t^0 = 29.2$ μs (line 4), which is one order larger than the induction length of $l_i = 1.49$ mm for mixture 1. Moreover, the peak pressure continuously decreases as the transmitted shock propagates downstream of the inert layer, which corresponds to continual attenuation of the leading shock speed after it passes across the inert layer. However, around $t - t^0 = 41$ μs (line 5), the first autoignition (A1) occurs and induces a rapid increase in both peak pressure and leading shock speed. At $t - t^0 = 64.6$ μs (line 7), the secondary autoignition (A2) happens. Consequently, detonation reinitiation is achieved and the leading shock speed abruptly accelerates at $t - t^0 = 72.3$ μs (line 8). The overdriven detonation forms and its peak pressure is around 6 atm, which is much higher than the pressure of the von Neumann spike of $P_{VN} = 3.9$ atm. At $t - t^0 = 95$ μs (line 10), the detonation is fully developed.

When the inert layer thickness is increased to $a = 8$ mm for mixture 1 (red line in Fig. 2a), Fig. 3b shows that the distance between the leading shock and the reaction front reaches 24.7 mm at $t - t^0 = 49.9$ μs (line 5 in Fig. 3b), which is much larger than 14.1 mm for mixture 1 with $a = 7$ mm, shown in Fig. 3a. Although autoignition occurs behind the leading shock at $t - t^0 = 67$ μs (line 6), the autoignition induced reaction front cannot couple with the leading shock. Consequently, there is no detonation reinitiation and the detonation is quenched by the inert layer.

When the nitrogen dilution is increased to $s = 7$ (mixture 4) while the inert layer thickness is still $a = 8$ mm (green line in Fig. 2b), the overall processes are similar to those in Fig. 3a and detonation reinitiation occurs. Different from the result for mixture 1 with $a = 8$ mm, Fig. 3c shows that the autoignition occurs at $t - t^0 = 55.4$ μs (line 6 in Fig. 3c). The autoignition-induced reaction front accelerates and couples with the leading shock at $t - t^0 = 84.4$ μs (line 9). This is because the leading shock speed is relatively small as compared to that for mixture 1, and thereby the reaction front can catch up with the leading shock more easily. Besides, the autoignition position is close to the leading shock, and their distance is around 6.1 mm, which is close to the induction length of $l_i = 4.31$ mm for mixture 2. Consequently, for the same inert layer thickness of $a = 8$ mm, successful detonation reinitiation occurs in mixture 2, which has higher dilution and longer induction length than mixture 1.

As depicted in Fig. 3a, there is a transition distance l_t after which the overdriven detonation develops. The transition distance is defined as the distance between the position where the inert layer starts to appear and the position where the sharp increase of shock speed occurs (i.e., the overdriven detonation develops). Figure 4 summarizes the change of the transition distance with the inert layer thickness from 1-D simulations, in which the dashed vertical lines correspond to the critical inert layer thickness. The transition distance is shown to increase with the inert layer thickness for both mixtures 1 and 4, which is consistent with experimental results in Ref. [15]. For larger inert layer thickness, the transmitted shock after the inert layer becomes weaker. Consequently, a longer transition distance is needed to induce autoignition in the unburned mixture compressed by the transmitted shock and to achieve successful detonation reinitiation. Moreover, Fig. 4 shows that nitrogen dilution slightly increases the transition distance, whereas it greatly increases the critical inert layer thickness from $a_c = 7$ mm for mixture 1 to $a_c = 10$ mm for mixture 2.

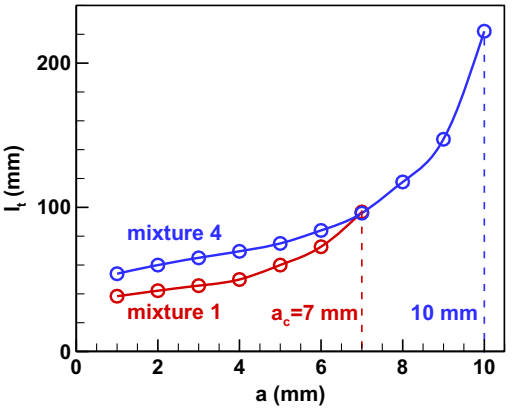

Fig. 4 Change of transition distance with the inert layer thickness from 1-D simulations.

In summary, the aforementioned 1-D results demonstrate that N_2 dilution increases the critical inert layer thickness. Similarly, the results on mixtures 4–6 (not shown here) indicate that the critical inert layer increases as the pressure decreases. This is because increasing N_2 dilution and reducing initial pressure both can increase the induction length (see Table 1), and thereby affect detonation propagation across an inert layer.

B. Two-Dimensional Detonation Propagation

Then, we considered the 2-D detonation propagating across an inert layer. Six mixtures with different amounts of N_2 dilution and/or at different initial pressures (see Table 1) were all considered, although the results for mixtures 1 and 4 are mainly discussed here.

Figure 5 shows the numerical soot foils (which are obtained by recording the maximum pressure history in the computational domain) for mixtures 1 and 4 and two inert layer thicknesses. Regular cellular structure is fully developed, and the peak pressure approaches to constant before the detonation enters the inert layer starting at $x = 0$ cm($\Delta x = 150 l_i$). After entering the inert layer, the pressure at the triple points decreases substantially, indicating that the reaction front starts to decouple with the leading shock. After passing the inert layer, the shock waves decay greatly and some triple points disappear, resulting in the formation of larger cells as shown in Fig. 5. A similar trend was also observed in Ref. [17]. For mixture 1 with the inert layer thickness of $a = 7$ mm, Fig. 5a shows that the peak pressure of

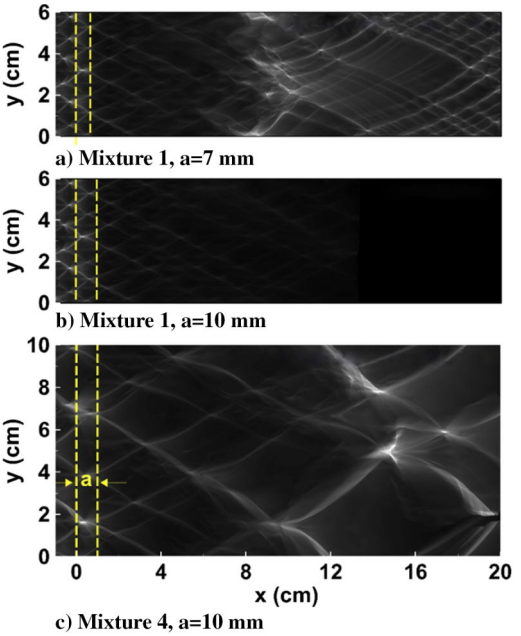

Fig. 5 Numerical soot foils for mixtures 1 and 4.

cellular structures decays rapidly and the triple points almost disappear for $0 < x < 6$ cm. Around $x = 9$ cm, local explosions occur and the peak pressure increases and reaches 21 atm. Detonation reinitiation happens and cellular structures with a relatively small size appear. Then, the cell size gradually increases; finally, the quasi-steady propagation is reached. When the inert layer thickness is increased to $a = 10$ mm, Fig. 5b shows that the detonation quenches after passing the inert layer and there is no detonation reinitiation. As nitrogen dilution increases (from mixture 1 with $H_2:O_2:N_2 = 2:1:3.76$ to mixture 4 with $H_2:O_2:N_2 = 2:1:7$), the cell size increases and the peak pressure of the cellular structure decreases as detonation propagates across inert layer. This indicates that detonation quenches. Thereafter, successful detonation reinitiation is achieved by local explosions occurring around $x = 11$ cm. Therefore, Fig. 5 indicates that the increase in nitrogen dilution results in larger critical inert layer thickness. This trend is the same as was observed for the 1-D case.

To show more details on detonation quenching and reinitiation processes, the evolution of temperature contours is plotted in Fig. 6, in which SRD denotes the shock–reaction front decoupling, SRC denotes the shock–reaction front coupling, and E denotes explosion. The mixtures and inert layers are the same as those in Fig. 5. The

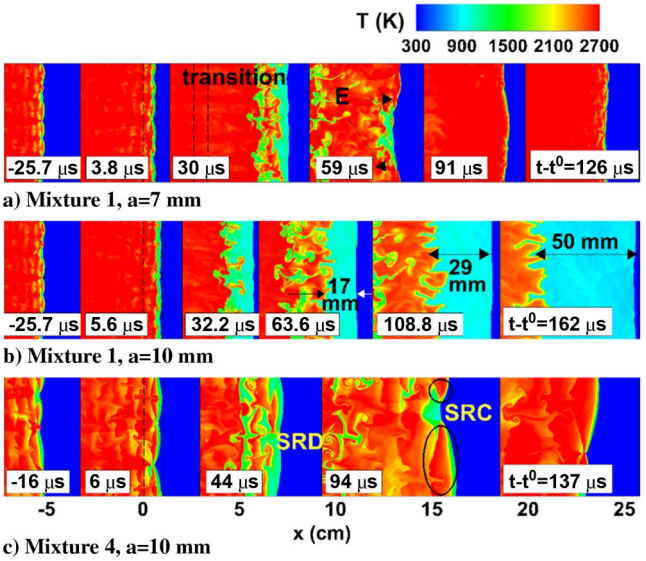

Fig. 6 Evolution of temperature contours for mixtures 1 and 4.

detonation enters the inert layer (dashed line at $x = 0$ cm) at $t - t_0 = 0$ μs. Before entering the inert layer, in the regular cellular structure, there is a relatively larger induction zone immediately after the incident shock because it is as weaker compared to the Mach stem. The "unburned pockets" in these induction zones are brought into the inert layer and are consumed there by chemical reactions afterward. The transmitted shock compresses the flammable mixture on the right side of the inert layer and increases its temperature to be above 1000 K, which induces local autoignition/explosion. Detonation reinitiation depends on whether an autoignition-induced reaction front couples with the transmitted shock. A comparison between Figs. 6a and 6b shows that the wider the inert layer, the longer the distance between the reaction front and the leading shock. Consequently, detonation reinitiation fails for the case with a thicker inert layer. For mixture 4 with $a = 10$ mm, Fig. 6c shows that the local autoignition-induced reaction front is able to couple with the leading shock, which results in successful detonation reinitiation.

To further demonstrate the autoignition process, Fig. 7 plots the evolution of the enlarged density gradient, pressure, and temperature contours for mixture 1 with $a = 7$ mm at $t - t_0 = -4$ μs (top row), 41 μs (middle row), and 56 μs (bottom row). In Fig. 7, M stands for the Mach stem, I stands for incident shock, T stands for transverse wave, R stands for Richtmyer–Meshkov instability, A stands for autoignition, and E stands for explosion. At $t - t^0 = -4$ μs (i.e., before the detonation enters the inert layer), the triple points consist of the incident shock I, the Mach stem M, and the transverse wave T. The reaction zone couples with the leading shock. As the detonation propagates across the inert layer, the leading shock collides with the interface between flammable H_2/air and inert nitrogen twice, which induces Richtmyer–Meshkov (RM) instabilities, R_1 and R_2, as indicated in Fig. 7 (see the density gradient contour at $t - t^0 = 41$ μs). After interacting with the interface, the incident leading shock splits into the transmitted and reflected shocks [14]. Besides, the density and acoustic impedance of the inert nitrogen are different from those of an H_2/air mixture, which changes the shock strength [36]. As shown by the temperature contour at $t - t^0 = 41$ μs, the reaction zone fully decouples with the leading shock and the distance between the reaction zone and the leading shock is much larger than the induction length. The wrinkled reaction front is induced by RM instabilities. Meanwhile, the interaction of transverse waves T_1 and T_2 and the RM instability R_2 results in the folding or superimposition of shock waves, which forms a local maximum of pressure and temperature, and thereby induces the autoignition A_1 and subsequent explosion E_1 at $t - t^0 = 41$ μs. The local explosion interacts with the transverse wave T_2, which induces new autoignition A_2 and local explosion E_2 at $t - t^0 = 56$ μs, as

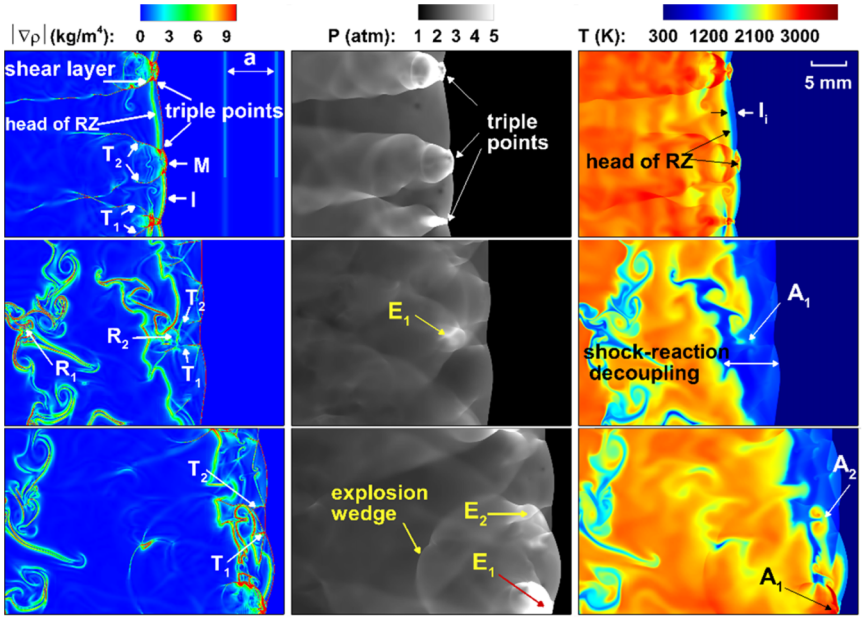

Fig. 7 Evolution of density gradient, pressure, and temperature contours for mixture 1 with $a = 7$ mm (RZ = reaction zone).

shown in Fig. 7. Local explosions spread over the entire domain and a global explosion forms (see Fig. 6a). Finally, successful detonation reinitiation is achieved for this case.

The preceding results demonstrate that when the inert layer thickness is below some critical value, successful detonation reinitiation is achieved after a transition process. To obtain the critical inert layer thickness a_c, detonation propagating across a single inert layer with different thicknesses is simulated. The results for mixture 1 are shown in Fig. 8.

The results for a homogenous mixture without inert layer (i.e., $a = 0$) are shown in Fig. 8 for comparison. For $a = 2$ mm, the inert layer has little influence on detonation propagation. The only difference is that the pressure at triple points slightly decreases after the inert layer. The cellular structure remains nearly the same as that for $a = 0$. When the inert layer thickness is increased to $a = 5$ mm, Fig. 8 shows that there is an obvious transition process: during which, both the number of triple points and the peak pressure decrease. For $a = 7$ and 8 mm, the cellular structures fully disappear during the transition process. For $a = 10$ mm, the detonation quenches without reinitiation. Note that the result for $a = 10$ mm is independent of the computational domain length: detonation failure still occurs when the domain is extended.

Figure 8 indicates that the transition distance increases with the inert layer thickness. The transition distance from 2-D simulations l_t is plotted in Fig. 9, which shows that l_t for the 2-D case is smaller than that for the 1-D case. This is because multidimensional effects (e.g., transverse waves and their interaction as shown in Fig. 7) can promote local autoignition and detonation reinitiation. Figures 4 and 9 show that the critical inert layer thicknesses are 7 and 8 mm, respectively, for the 1-D and 2-D cases in mixture 1; and they are 10 and 20 mm, respectively, for 1-D and 2-D cases in mixture 4. This

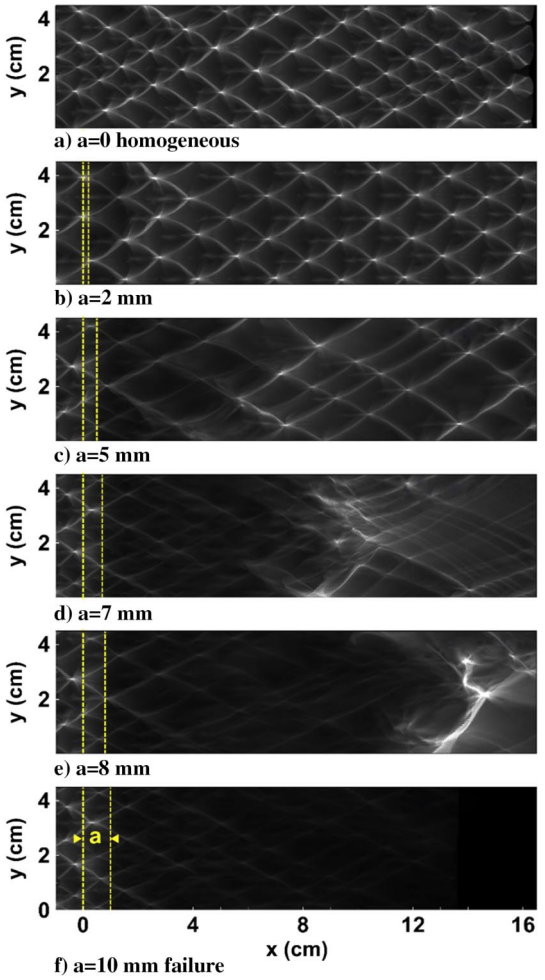

Fig. 8 Numerical soot foils for mixture 1 with different inert layer thicknesses.

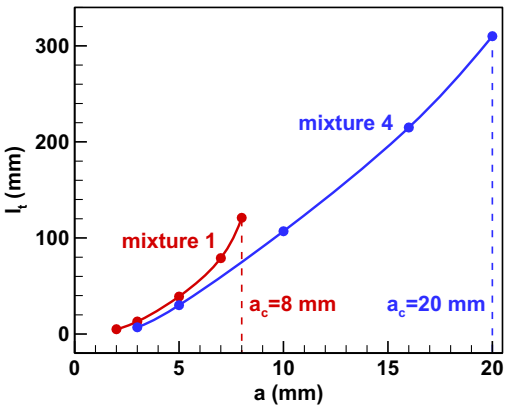

Fig. 9 Change of transition distance with the inert layer thickness from 2-D simulations.

is because in the 1-D case, only the transmitted normal shock helps to induce detonation reinitiation; whereas in the 2-D case, the interaction among the Mach stem, the transverse wave, and the incident shock wave greatly promotes local autoignition/exposition, and thereby enhances detonation reinitiation. Besides, from Fig. 9, we observed that the differences for both the transition distance and the critical inert layer become larger as the amount of N_2 dilution increases (from mixture 1 in red lines to mixture 4 in blue lines). This indicates that the effects of the transverse wave on detonation transmission increase with the amount of N_2 dilution.

The preceding results show that nitrogen dilution increases the critical inert layer a_c. Similarly, decreasing the initial pressure also increases a_c. Figure 10 shows a_c as a function of detonation cell size for the six mixtures listed in Table 1. The line is a linear fit. Because the density of the inert layer is different from that of the reactive mixture, there is a change in shock impedance. We introduce an artificial inert mixture, $H_2 * /O_2 * /N_2*$, which has the same thermal properties and acoustic impedance as the reactive $H_2/O_2/N_2$ mixture. Figure 10 also shows the results for an inert layer consisting of an artificial inert mixture, $H_2*/O_2*/N_2*$. With the increase of nitrogen dilution (i.e., mixture $1 \rightarrow 2 \rightarrow 3 \rightarrow 4$ in Fig. 10) or the decrease of initial pressure (i.e., mixture $6 \rightarrow 5 \rightarrow 4$), both the critical inert layer thickness and the detonation cell size increase. Therefore, the critical inert layer thickness is positively correlated to the detonation cell size or detonation induction length. Similar to the 1-D case, the aforementioned 2-D results also demonstrate that for a larger cell size or induction length resulting from the higher nitrogen dilution or lower initial pressure, the self-sustained detonation can propagate under the condition in which the reaction zone is relatively away from the leading shock. This is the benefit of detonation propagating across an inert layer, and thus the larger critical inert layer thickness is obtained. Besides, Fig. 10 shows that the critical inert layer thickness for the inert layer with the artificial mixture $H_2 * /O_2 * /N_2*$ is close to that

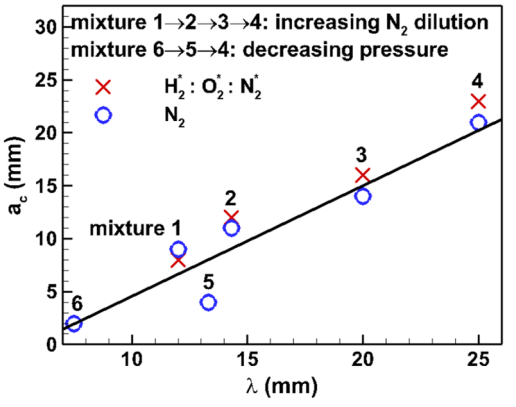

Fig. 10 Critical inert layer thickness and cell size for mixtures listed in Table 1.

for an inert layer of pure nitrogen. Therefore, the change of acoustic impedance across the inert layer has little influence on detonation transition, at least for the cases consider in this work.

In the present work, the cell size based on the detailed chemistry [23] is much smaller than the measured values in the experiments [37]. However, the qualitative relationship between the critical inert layer thickness and the cell size/induction length can be obtained. Besides, the present work only conducted 1-D and 2-D simulations; three-dimensional (3-D) cases will allow additional interaction among shock waves.

IV. Conclusions

Detonation propagation across an inert layer was investigated through one- and two-dimensional simulations considering detailed chemistry for stoichiometric $H_2/O_2/N_2$ mixtures. Six mixtures with different amounts of nitrogen dilution and at different initial pressures were considered. This work focuses on assessing the effects of an inert layer on detonation transmission, especially the autoignition/explosion and detonation reinitiation processes. After the detonation enters the inert layer, the reaction front starts to decouple from the leading shock, and some triple points disappear. The cellular structures fully disappear if the inert layer thickness is large enough. Successful detonation reinitiation occurs downstream when the inert layer thickness is below some critical value, i.e., $a < a_c$. The interaction of transverse waves, the reactive–inert layer interface, and the instabilities jointly induce local autoignition/explosion and detonation reinitiation.

The nitrogen dilution and initial pressure greatly affect the detonation propagating across the inert layer. The critical inert layer thickness was found to be positively correlated to the detonation cell size or induction length. With the increase of nitrogen dilution or decrease of initial pressure, the induction length and cell size of detonation become larger, which unexpectedly results in the larger critical inert layer thickness. Therefore, counterintuitively, a thicker inert layer is required to quench a weaker detonation (with more nitrogen dilution or with lower-energy density at lower pressure). Moreover, the critical inert layer thickness for the 1-D case was found to be lower than that for the 2-D case because interaction among shock waves occurring in the 2-D case rather than the 1-D case promotes local autoignition/exposition.

It is noted that the simplified model considered here is far from the practical cases using inert layers to quench detonations. For example, the inert gas is not static, and it mixes with the flammable gases. The present mixture has a regular detonation cell structure. For detonations with an irregular cell structure, the reinitiation after passing an inert layer might be easier. These need to be explored in future studies. Besides, periodic boundary conditions in the direction normal to the detonation propagation were used in this study. As mentioned before, in practice, the detonation propagates in a finite domain with physical confinement. Therefore, in future works, it would be interesting to take into account the confinement effect. Furthermore, there exists the third dimension that allows additional interaction among shock waves. The effects of inert layers on detonation propagation need to be studied through 3-D simulations in future works. Besides, in real propulsion systems, there is strong turbulence that might affect the detonation structure (e.g., to broaden the reaction zone) as well as the inert layer. Consequently, the interaction between the detonation and the interlayer is affected by the turbulence. The dependence of the critical inert layer thickness and detonation reinitiation on the turbulence intensity needs to be investigated in future works.

Acknowledgment

This work was supported by the National Natural Science Foundation of China (no. 52176096).

References

[1] Abdin, Z., Zafaranloo, A., Rafiee, A., and Khalilpour, K., "Hydrogen as an Energy Vector," *Renewable and Sustainable Energy Reviews*, Vol. 120, March 2020, Paper 109620. https://doi.org/10.1016/j.rser.2019.109620

[2] Sánchez, A. L., and Williams, F. A., "Recent Advances in Understanding of Flammability Characteristics of Hydrogen," *Progress in Energy and Combustion Science*, Vol. 41, 2014, pp. 1–55. https://doi.org/10.1016/j.pecs.2013.10.002

[3] Han, W., Huang, J., and Wang, C., "Pulsating and Cellular Instabilities of Hydrogen–Oxygen Detonations with Ozone Sensitization," *Physics of Fluids*, Vol. 33, No. 7, 2021, Paper 076113.

[4] Xu, Y., Zhao, M., and Zhang, H., "Extinction of Incident Hydrogen/Air Detonation in Fine Water Sprays," *Physics of Fluids*, Vol. 33, 2021, Paper 116109. https://doi.org/10.1063/5.0055080

[5] Chen, X., Bttler, H., Scholtissek, A., Hasse, C., and Chen, Z., "Effects of Stretch-Chemistry Interaction on Chemical Pathways for Strained and Curved Hydrogen/Air Premixed Flames," *Combustion and Flame*, Vol. 232, 2021, Paper 111532. https://doi.org/10.1016/j.combustflame.2021.111532

[6] Zhang, W., Kong, W., Sui, C., Wang, T., and Peng, L., "Effect of Hydrogen-Rich Fuels on Turbulent Combustion of Advanced Gas Turbine," *Journal of Thermal Science*, Vol. 31, No. 2, 2022, pp. 561–570. https://doi.org/10.1007/s11630-021-1539-8

[7] Zhang, F., Zirwes, T., Wang, Y., Chen, Z., Bockhorn, H., Trimis, D., and Stapf, D., "Dynamics of Premixed Hydrogen/Air Flames in Unsteady Flow," *Physics of Fluids*, Vol. 34, 2022, Paper 085121. https://doi.org/10.1063/5.0098883

[8] Chen, X., Xie, S., Böttler, H., Scholtissek, A., Han, W., Yu, D., Hasse, C., and Chen, Z., "Effects of Electrodes and Imposed Flow on Forced Ignition in Laminar Premixed Hydrogen/Air Mixtures with Large Lewis Number," *Proceedings of the Combustion Institute*, Sept. 2022.

[9] Abohamzeh, E., Salehi, F., Sheikholeslami, M., Abbassi, R., and Khan, F., "Review of Hydrogen Safety During Storage, Transmission, and Applications Processes," *Journal of Loss Prevention in the Process Industries*, Vol. 72, No. 3, 2021, Paper 104569. https://doi.org/10.1016/j.jlp.2021.104569

[10] Yang, F., Wang, T., Deng, X., Dang, J., Huang, Z., Hu, S., Li, Y., and Ouyang, M., "Review on Hydrogen Safety Issues: Incident Statistics, Hydrogen Diffusion," *International Journal of Hydrogen Energy*, Vol. 46, 2021, pp. 31467–31488. https://doi.org/10.1016/j.ijhydene.2021.07.005

[11] Kuznetsov, M., Denkevits, A., Veser, A., and Friedrich, A., "Flame Propagation Regimes and Critical Conditions for Flame Acceleration and Detonation Transition for Hydrogen-Air Mixtures at Cryogenic Temperatures," *International Journal of Hydrogen Energy*, Vol. 47, No. 71, 2022, pp. 30,743–30,750. https://doi.org/10.1016/j.ijhydene.2022.07.024

[12] Mi, X., Higgins, A. J., Ng, H. D., Kiyanda, C. B., and Nikiforakis, N., "Propagation of Gaseous Detonation Waves in a Spatially Inhomogeneous Reactive Medium," *Physical Review Fluids*, Vol. 2, No. 5, 2017, Paper 053201. https://doi.org/10.1103/PhysRevFluids.2.053201

[13] Teodorczyk, A., and Benoan, F., "Interaction of Detonation with Inert Gas Zone," *Shock Waves*, Vol. 6, 1996, pp. 211–223. https://doi.org/10.1007/BF02511378

[14] Bull, D. C., Elsworth, J. E., McLeod, M. A., and Hughes, D., "Initiation of Unconfined Gas Detonations in Hydrocarbon-Air Mixtures by a Sympathetic Mechanism," *Progress in Astronautics and Aeronautics*, Vol. 75, 1980, pp. 61–72. https://doi.org/10.2514/5.9781600865497.0061.0072

[15] Bjerketvedt, D., Sonju, O. K., and Moen, I. O., "The Influence of Experimental Condition on the Reinitiation of Detonation Across an Inert Region," *Progress in Astronautics and Aeronautics*, Vol. 106, 1986, pp. 109–130. https://doi.org/10.2514/5.9781600865800.0109.0130

[16] Tropin, D., and Bedarev, I., "Physical and Mathematical Modeling of Interaction of Detonation Waves with Inert Gas Plugs," *Journal of Loss Prevention in the Process Industries*, Vol. 72, 2021, Paper 104595. https://doi.org/10.1016/j.jlp.2021.104595

[17] Tang-Yuk, K. C., Mi, X. C., and Lee, J. H. S., "Transmission of a Detonation Wave Across an Inert Layer," *Combustion and Flame*, Vol. 236, 2022, Paper 111769. https://doi.org/10.1016/j.combustflame.2021.111769

[18] Wang, Y., Huang, C., Deiterding, R., Chen, H., and Chen, Z., "Propagation of Gaseous Detonation Across Inert Layers," *Proceedings of the Combustion Institute*, Vol. 38, No. 3, 2021, pp. 3555–3563. https://doi.org/10.1016/j.proci.2020.07.022

[19] Chen, Z., Burke, M. P., and Ju, Y., "Effects of Lewis Number and Ignition Energy on the Determination of Laminar Flame Speed Using

Propagating Spherical Flames," *Proceedings of the Combustion Institute*, Vol. 32, No. 1, 2009, pp. 1253–1260. https://doi.org/10.1016/j.proci.2008.05.060

[20] Chen, Z., "Effects of Radiation and Compression on Propagating Spherical Flames of Methane/Air Mixtures near the Lean Flammability Limit," *Combustion and Flame*, Vol. 157, No. 12, 2010, pp. 2267–2276. https://doi.org/10.1016/j.combustflame.2010.07.010

[21] Deiterding, R., "Block-Structured Adaptive Mesh Refinement-Theory, Implementation and Application," *ESAIM: Proceedings*, Vol. 34, Dec. 2011, pp. 97–150. https://doi.org/10.1051/proc/201134002

[22] Deiterding, R., "High-Resolution Numerical Simulation and Analysis of Mach Reflection Structures in Detonation Waves in Low-Pressure $H_2 - O_2$-Ar Mixtures: A Summary of Results Obtained with the Adaptive Mesh Refinement Framework AMROC," *Journal of Combustion*, Vol. 2011, 2011, pp. 1–18. https://doi.org/10.1155/2011/738969

[23] Li, J., Zhao, Z., Kazakov, A., and Dryer, F. L., "An Updated Comprehensive Kinetics Model of Hydrogen Combustion," *International Journal of Chemical Kinetics*, Vol. 36, 2004, pp. 566–575. https://doi.org/10.1002/kin.20026

[24] Zhao, W., Liang, J., Deiterding, R., Cai, X., and Wang, X., "Effect of Transverse Jet Position on Flame Propagation Regime," *Physics of Fluids*, Vol. 33, 2021, Paper 091704. https://doi.org/10.1063/5.0063363

[25] Huang, C., Wang, Y., Deiterding, R., Yu, D., and Chen, Z., "Numerical Studies on Weak and Strong Ignition Induced by Reflected Shock and Boundary Layer Interaction," *Acta Mechanica Sinica*, Vol. 38, 2022, Paper 121466. https://doi.org/10.1007/s10409-021-09011-x

[26] Luan, Z., Huang, Y., Deiterding, R., and You, Y., "On the Evolutions of Triple Point Structure in Wedge-Stabilized Oblique Detonations," *Physics of Fluids*, Vol. 34, 2022, Paper 067118. https://doi.org/10.1063/5.0090975

[27] Wang, Y., Movaghar, A., Wang, Z., Liu, Z., and Chen, Z., "Laminar Flame Speeds of Methane/Air Mixtures at Engine Conditions: Performance of Different Kinetic Models and Power-Law Correlations," *Combustion and Flame*, Vol. 218, 2020, pp. 101–108. https://doi.org/10.1016/j.combustflame.2020.05.004

[28] Su, J., Wu, Y., Wang, Y., Chen, X., and Chen, Z., "Skeletal and Reduced Kinetic Models for Methane Oxidation Under Engine-Relevant Conditions," *Fuel*, Vol. 288, 2021, Paper 119667. https://doi.org/10.1016/j.fuel.2020.119667

[29] Wang, Y., Chen, Z., and Chen, H., "Propagation of Gaseous Detonation in Spatially Inhomogeneous Mixtures," *Physics of Fluids*, Vol. 33, No. 11, 2021, Paper 116105. https://doi.org/10.1016/j.combustflame.2021.02.040

[30] Wang, Y., Han, W., and Chen, Z., "Effects of Stratification on Premixed Cool Flame Propagation and Modeling," *Combustion and Flame*, Vol. 229, 2021, Paper 111394. https://doi.org/10.1016/j.combustflame.2021.02.040

[31] Sato, T., and Raman, V., "Detonation Structure in Ethylene/Air-Based Non-Premixed Rotating Detonation Engine," *Journal of Propulsion and Power*, Vol. 36, No. 5, 2020, pp. 752–762. https://doi.org/10.2514/1.b37664

[32] Pal, P., Demir, S., and Som, S., "Numerical Analysis of Combustion Dynamics in a Full-Scale Rotating Detonation Rocket Engine Using Large Eddy Simulations," *Journal of Energy Resources Technology*, Vol. 145, No. 2, 2022, pp. 1–31. https://doi.org/10.1115/1.4055206

[33] Ng, H. D., and Lee, J. H. S., "Direct Initiation of Detonation with a Multi-Step Reaction Scheme," *Journal of Fluid Mechanics*, Vol. 476, 2003, pp. 179–211. https://doi.org/10.1017/s0022112002002872

[34] Qi, C., and Chen, Z., "Effects of Temperature Perturbation on Direct Detonation Initiation," *Proceedings of the Combustion Institute*, Vol. 36, No. 2, 2017, pp. 2743–2751. https://doi.org/10.1016/j.proci.2016.06.093

[35] Faghih, M., Mével, R., He, Y., and Chen, Z., "Effect of 2-Step Energy Release on Direct Detonation Initiation by a Point Energy Source in a Rich $H_2 - NO_2/N_2O_4$ Mixture," *Combustion and Flame*, Vol. 222, 2020, pp. 317–325. https://doi.org/10.1016/j.combustflame.2020.08.036

[36] Ishii, K., and Seki, K., "A Study on Suppression of Detonation Propagation by Inert Gas Injection," *Proceedings of the 26th International Colloquium on the Dynamics of Explosions and Reactive Systems*, 2017, Paper 1031, http://www.icders.org/ICDERS2017/abstracts/ICDERS2017-1031.pdf.

[37] Kaneshige, M., and Shepherd, J. E., "Detonation Database," FM97-8, GALCIT, July 1997, https://authors.library.caltech.edu/25827/.

L. Qiao
Associate Editor